Simulation of *p-n* junctions: Present and future challenges for technologies beyond 32 nm

Lourdes Pelaz,[a)] Luis A. Marqués, María Aboy, Iván Santos, and Pedro López
Universidad de Valladolid, Campus Miguel Delibes, 47011 Valladolid, Spain

Ray Duffy
NXP-TSMC Research Center, Kapeldreef 75, 3001 Leuven, Belgium

(Received 15 June 2009; accepted 24 August 2009; published 1 March 2010)

Ion implantation continues being the dominant technique to introduce dopants in Si devices. With the device feature size in the nanometer scale, the accurate and detailed description of as-implanted dopant and damage profiles is becoming key as advanced annealing techniques are almost diffusionless. The demanding requirements for ultrashallow junction formation are stimulating the development of improved and detailed models for molecular implants and for the kinetics of amorphous damage. Additional challenges arise in the doping of advanced architectures, such as fin field effect transistors, because the introduction of highly tilted ions is quite inefficient and, in addition, the regrowth of amorphous regions in narrow structures is hampered by the slow regrowth at free interfaces and {111} planes. Atomistic simulations play a relevant role to provide the understanding for the development of simplified physically based models computationally more efficient. © *2010 American Vacuum Society.* [DOI: 10.1116/1.3231481]

I. INTRODUCTION

As devices are scaled down, it is becoming more and more challenging to keep a good control of short channel effects (SCEs) with simultaneous high drive currents and low off-state leakage.[1] At the junction level, the need to control SCE has motivated the progressive reduction in junction depth at the source and drain (S/D) extensions. Junctions are generally formed by ion implantation as this is a conventional and well established technique. The formation of ultrashallow junctions is particularly challenging in the case of B because its low mass demands the use of ultralow energy implants. Molecular implants with $B_{18}H_{22}$ ions have proven to be advantageous for ultrashallow junction formation because higher extraction energy can be used while the effective energy per B ion is scaled by the number of B atoms in the molecule.[2] In addition, the damage created by this heavy molecule causes self-amorphization, saving the preamorphization implant step required when monoatomic B is used to take advantage of solid-phase epitaxial regrowth (SPER). The maximization of drive current for higher switching speed demands a minimization of access resistance. This requirement has driven the development of strain technologies to enhance carrier mobility[3] and the use of SPER and millisecond anneals to achieve maximum dopant activation with minimal diffusion.[4] However, the presence of residual defects after regrowth is a pressing concern as they can cause additional leakage, limiting low power applications. The removal of these defects generally requires high thermal budgets, which causes the spreading of the junction depth, and therefore, deteriorates SCE control. The difficult trade-off between shallow junction formation, maximum dopant activation, and defect removal becomes more and more challenging as the gate length is reduced further in each technology node.[1] To be able to maintain a good SCE control while fulfilling other device requirements, the International Technology Roadmap for Semiconductors foresees a transition from traditional planar silicon metal oxide semiconductor (MOS) field effect transistors to ultrathin-body fully depleted MOS devices in the near future and to alternative device architectures, such as fin field effect transistors (FinFETs), at the 22 nm node and beyond.[1] The incorporation of materials with very high carrier mobility, such as Ge and III-V compounds, to substitute Si in the channel of advanced device architectures is being considered for further technologies.[1,5]

The goal of process modeling is to provide physical understanding and simulation tools to help the development and optimization of device fabrication. Therefore, the trends in device technology drive the requirements for process modeling. (i) The continuous reduction in feature size in the devices is demanding improved models so that small variations in the dopant profiles can be accurately predicted. Kinetic Monte Carlo (KMC) methods are starting to play a more relevant role as they can reach actual device dimensions and time scales typical of actual processes. (ii) For new device architectures, it is necessary to assess existing processes and probably develop new ones to address new issues that arise in nonplanar structures. (iii) The incorporation of other materials, such as Ge or III-V compounds, to substitute Si in the channel, is promoting a number of studies to establish models and parameters that describe accurately the behavior of dopants and defects in these materials during process integration in nanometer scale high speed logic devices.

For the models to be able to fulfill their goal, they should be physically based and computationally efficient. Theory and dedicated experiments provide information about fundamental mechanisms and parameters. However, the resulting models may be computationally too expensive to be effec-

[a)]Electronic mail: lourdes@ele.uva.es

tively used for device optimization. Empirical approaches and fitting are sometimes used to develop simplified models that are computationally efficient and accurate, at least within a limited and relevant range of process parameters. Simplified models can also be extracted from the understanding of the most relevant mechanisms that take place through a multiscale approach.[6] *Ab initio* methods are parameter free and include the quantum description of the atomic system, but due to its huge computational load, only a few atoms (64–216) are typically included in the simulations. Classical molecular dynamics (MD) describes the dynamics of the atoms based on empirical classical potentials. Although the Si–Si interaction is reasonably well described by empirical potentials,[7–9] no good empirical classical potentials have been established to capture the interaction between Si and impurities. Typical simulation cells include between 10^3 and 10^6 atoms, but this technique is very time consuming for simulation times above 1 ps. It is useful to extract mechanisms and atomic parameters that can be used in the other less detailed techniques. Atomistic simulations that reach sizes typical of actual devices (10–100 nm) can be performed with KMC models. Their main drawback is the large number of atomistic parameters that must be specified, most of which are difficult to extract. Continuum models are based on the resolution of partial differential equations. They are the mainstream in process simulation because they incorporate many coupled processes (implantation, anneals, stress, oxidation, deposition steps, etc.) by using efficient simplified models.

In this article, we will provide an overview of the present status of ion implantation and annealing modeling, with special emphasis on atomistic models. By using atomistic simulation techniques, we will also address relevant doping issues that arise in nonplanar geometries.

II. MODELING OF ION IMPLANTATION AND ANNEALING

Ion implantation remains the stronger candidate as a mean to introduce dopants because it allows a good control of the dopant profile. However, the demanding requirements to form ultrashallow junctions are bringing about new issues. Molecular implants are being considered as a way to introduce dopant atoms very close to the surface.[2] Implants at temperatures well below room temperature or at elevated temperatures are being investigated to minimize residual damage.[10] As the device dimensions are reduced and millisecond anneals are almost diffusionless, an accurate prediction of the as-implanted dopant and damage profiles is becoming more relevant. Traditionally, the emphasis lied on the dopant profile since for nonamorphizing implants the "+1 model"[11] or "+*n* model"[12] were assumed for defects. However, the use of amorphizing implants followed by SPER calls for improved models for damage accumulation including damage kinetics, amorphization, and regrowth.

Although analytic functions are commonly used to describe one-dimensional dopant and damage profiles in fast continuum simulations,[13] the need to properly account for dopant fluctuations in small devices and the intrinsic two- and three-dimensional nature of advanced device architectures are demanding complex models to describe the implant profiles.[14] A good compromise between computer efficiency and detailed description is provided by binary collision approximation (BCA)-based Monte Carlo (MC) simulators.[15–19] BCA assumes that the energetic atom only interacts with one target atom at the time, transferring to it some of its energy. If the target atom receives more energy than a threshold value (between 15 and 20 eV for Si), the atom is extracted from its lattice position, generating a Frenkel pair (Si interstitial and vacancy) and starting a new recoil. If the energy received by target atoms is lower than the threshold value, it is generally assumed to be lost to phonons. BCA-based MC simulators properly calibrated give very accurate description of dopant profiles and an acceptable description of atomistic damage created by light ions. However, for heavy and molecular ions, the complexity of the generated damage is not properly described by these traditional models.[20] Other BCA-based MC simulators only follow the trajectory of incoming ions but not that of the recoils providing the atomic position of ions but a statistical, rather than atomistic, approach of the generated damage based on Kinchin–Pease models.[21]

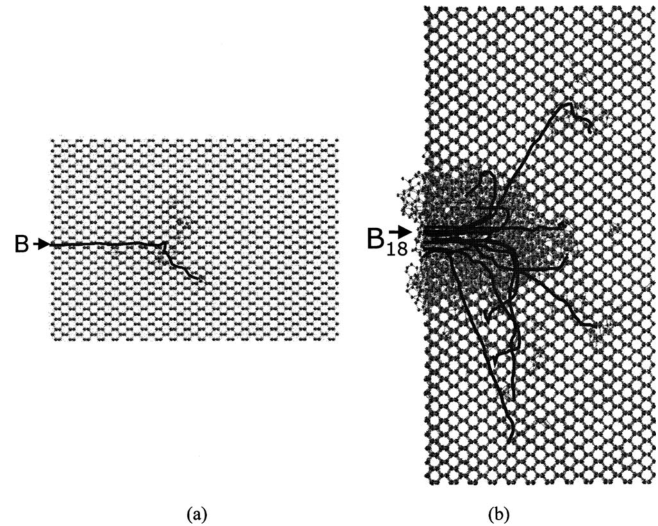

FIG. 1. Molecular dynamics simulations of the damage generated by (a) 0.5 keV monatomic B cascade and (b) 9 keV (0.5 keV per B atom) molecular B_{18} cascade.

The detailed damage description provided by MD can be used to understand the mechanisms involved in damage generation[20,22,23] and to set the basis for simplified models.[24,25] MD calculations indicate that, in the case of light ions, the interaction between energetic ions and target atoms is mostly ballistic, resulting in a dilute distribution of Si interstitials and vacancies and very small defect clusters, as shown in Fig. 1(a) for a 0.5 keV B implant. However, the damage resulting from implants with heavy molecules, such as $B_{18}H_{22}$, is significantly different from that corresponding to the superposition of the damage generated by individual B cascades. For equivalent energy per B atom (0.5 eV), on

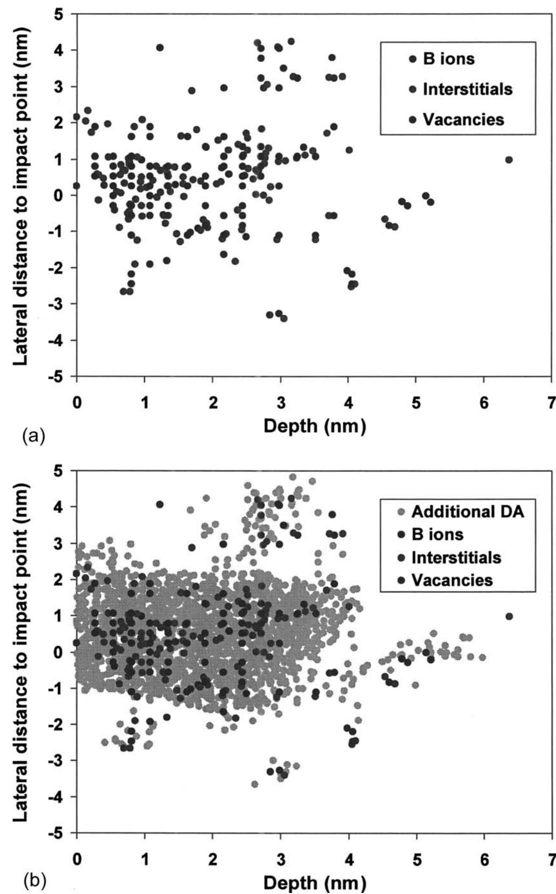

FIG. 2. Binary collision approximation–Monte Carlo based simulation of the damage generated by 18 simultaneous 0.5 keV B cascades using (a) classical atomistic damage model that generates Si interstitials and vacancies and (b) improved model that includes also the additional displaced atoms due to the energy transfers below the threshold value.

average, 32 atoms are displaced with respect to their lattice positions in the case of monoatomic B implants, while in the case of B_{18} implants, each B atom produces, on average, 108 displaced Si atoms. In this case, the main damage generation mechanism is the local melting of the region where a high amount of energy is simultaneously deposited by the B atoms.[22] This mechanism causes a huge amorphous region (*a*-region) around the impact point, as shown in Fig. 1(b). These ideas derived from MD simulations have been used to develop an improved model using the BCA-MC approach.[24] The model takes into account the energy transfers below the threshold value to account for the damage generated through melting. The resulting damage is a function not only of the total deposited energy but also of the local number of atoms in which the energy is deposited. This approach provides an atomistic description of the damage generated by molecular implants, not available to the date, with only a small additional computational load compared to traditional BCA models. The simulated damage generated by B_{18} implant using traditional BCA and improved BCA models are compared in Fig. 2. While traditional BCA models only produces Si interstitials and vacancies corresponding to 18 overlapping B

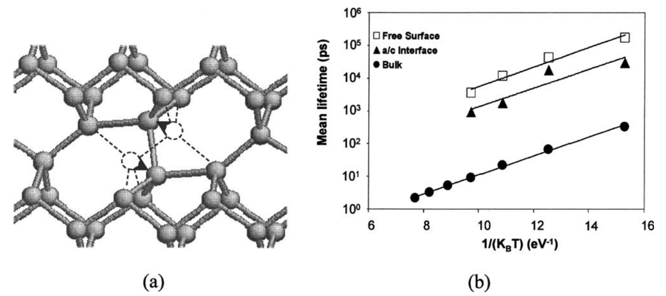

FIG. 3. (a) Structure of the bond defect or IV pair. (b) Arrhenius plot of the calculated mean lifetime of the bond defect when it is located at in bulk (surrounded by perfect crystalline Si), next to an amorphous/crystalline interface, and at a freestanding surface.

cascades, the improved BCA model generates significantly more damage at the center of the collision cascades, as it is predicted by MD simulations.

To describe the formation of *a*-regions, empirical approaches assume that the lattice becomes amorphous when the concentration of point defects (Si interstitials or vacancies) reaches a certain threshold, typically of the order of 2×10^{22} cm^{-3}.[26] This value is fitted by comparison with experimental results but it depends on ion mass, implant temperature and ion flux as a result of the dynamic annealing of the defects during the implantation.[27] The different annealing behaviors of the damage generated by different ions and the kinetics of crystalline to amorphous transition has been properly modeled using the bond defect or IV pair as the building block to describe the amorphous phase.[26] This defect, whose structure is represented in Fig. 3(a), is formed during ion implantation or by incomplete Si interstitial-vacancy recombination. It is assumed to recombine faster when it is surrounded by a larger number of Si atoms in crystalline lattice sites because these set a template for the lattice around the defect, favoring its recombination. The Arrhenius plot of the calculated average lifetime of isolated bond defects in a crystalline Si matrix and bond defects at an amorphous/crystalline interface and at a free interface is shown in Fig. 3(b). It indicates that bond defects at interfaces recombine over two orders of magnitude slower than isolated IV pairs in bulk. This explains the formation of near-surface *a*-regions with B at fluency much lower than those required to amorphize the volume.[28] The damage generated by ultralow energy implants, even with B, can easily accumulate near the interface and extend from there. The slower recombination of bond defects at the interfaces has also consequences for the recrystallization of narrow Si layers,[29,30] as we will illustrate later in the case of FinFETs.

Physically based models that properly describe mechanisms involved in the evolution of dopants in amorphous Si (*a*-Si) are not as well developed as they are in crystalline Si (*c*-Si). The interaction between dopants and defects in *c*-Si to account for dopant enhanced diffusion and clustering is well understood and characterized, both at experimental and theoretical levels (see Ref. 31 for a review). Detailed and simplified models have been developed for most common dopants used in Si processing. The study of dopants and

impurities, in general, in *a*-Si is much more complex than in *c*-Si. Since regrowth occurs quite fast at relatively low temperatures, the experimental window is quite limited, and the inherent diversity of local environments in an amorphous cell makes theoretical studies difficult. There are some empirical and quite simplistic models that account for some experimental observations but they lack physical basis that account for the rich phenomenological observations of dopants in *a*-Si.[32,33] B diffusion and clustering has been experimentally evidenced in B profiles in preamorphized Si.[34–36] Theoretical calculations have shown that there are some B cluster configurations that are energetically favorable to be formed during regrowth of *a*-Si.[37] Some models assume B clustering as the initial condition after regrowth when the B concentration exceeds the threshold concentration of the order of 2×10^{20} cm^{-3}.[32] However, it has been experimentally demonstrated that the threshold concentration for B clustering formation in *a*-Si increases when the regrowth occurs at high temperatures.[38] Other dopants, such as As, do not diffuse appreciably in *a*-Si (Ref. 39) but they exhibit a strong segregation during regrowth so that the dopant profile after regrowth significantly differs from the as-implanted one.[40] The incorporation of F in *a*-Si has been proven to be beneficial for ultrashallow junction formation because F-vacancy complexes appear in the regrown layer.[41] Some theoretical calculations have demonstrated the stability of some small F-vacancy complexes,[42] but also rather large complexes have been experimentally observed.[43] It would be necessary to develop physically based models that can provide the understanding and the clues required to optimize electrically active dopant profiles when SPER is involved.

III. DOPANT INCORPORATION AND DAMAGE RECOVERY IN FINFETS

To achieve a good control of SCE and off-state leakage, the fin widths of FinFET devices must be narrow[44,45] but the parasitic source-drain resistance increases as the fin width is scaled.[46,47] This challenge to optimize FinFET performance is complicated by the difficulties to dope the fin due to its vertical structure. Ion implantation remains a strong candidate to incorporate dopants,[48] although other techniques such as vapor phase doping[49] or plasma doping[50] are being considered as means to introduce dopants in FinFET devices. While predictive models exists for ion implantation, that is not the case for other emerging doping techniques. In this section, we will analyze some process issues that arise for junction formation in FinFETs by using ion implantation.

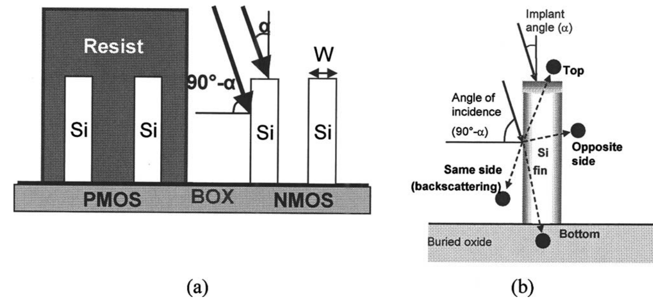

FIG. 4. (a) Schematic of the implant in dense fin arrays structures to illustrate the angle limitation. (b) Schematic of the different mechanisms of ion loss in a narrow fin structure.

One of the challenges in these devices is the inefficient dopant incorporation into the sidewalls of these vertical structures.[47,48,51] Tilted implants are used for that purpose but there is an angle restriction to avoid shadowing during implant of dense fin pitches. The fin height-to-spacing ratio and the resist height determine the maximum implant angle so that the ion beam hits the foot of each fin, as illustrated in Fig. 4(a). Using BCA-MC code MARLOWE,[15] we have evaluated the dopant incorporation for low and medium energy B and As ions implanted with different tilt angles in 10 nm wide fins. The schematic of the different mechanisms of dopant losses are shown in Fig. 4(b). The incident ion can be reflected at the incident interface and also some of the ions that penetrate into the Si could define a trajectory that ends up out of the fin. The percentage of ions retained and lost through the different mechanisms is plotted in Fig. 5 for 10° and 45° implants. In general, for a given implant angle and

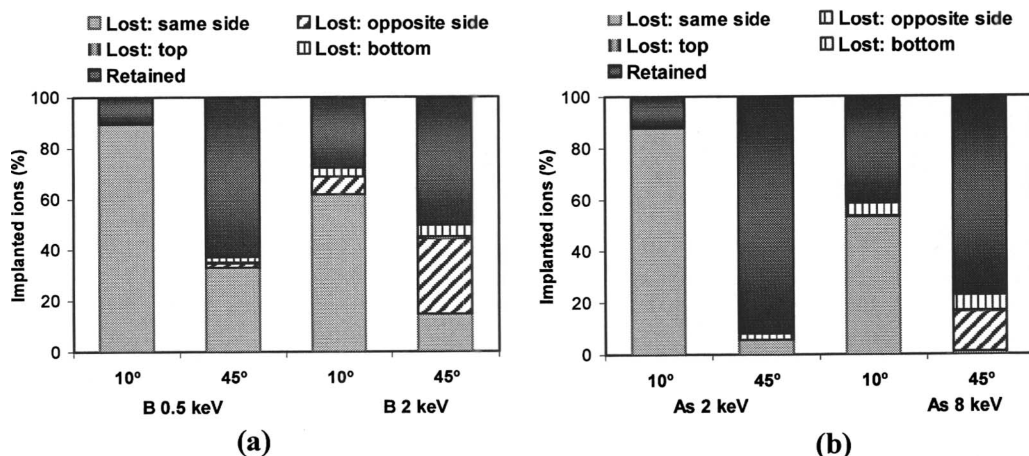

FIG. 5. Simulated percentage of ions implanted and quantification of the different sources of dopant loss for (a) B implants and (b) As implants into 10 nm wide fins.

projected range, heavier ions are better for dose retention. For 10° implants (80° implants to the sidewall), only a small fraction of ions is incorporated into the fin. Ion backscattering is responsible for most ion loss at low energies. At 45°, the amount of retained dose is significantly higher than that for 10° implants as ion backscattering is greatly reduced. However, when higher implant energies are used, the fraction of retained ions inside the fin decreases because the ion trajectory may escape from fin dimensions. The experimental verification of the inefficient incorporation of dopants when used highly tilted implants has been demonstrated by secondary ion mass spectroscopy analysis performed in blanket wafers[51] and fin structures.[52] The inefficient dopant incorporation, along with geometrical considerations,[53] causes a significant nonconformality in the dopant distribution (dopant concentration at the top surface much higher than in the sidewalls) that deteriorates the device performance.[45,52,54]

Another relevant issue in FinFETs is the damage removal and proper regrowth. Due to the narrowness of these structures, interfaces play a significant role in the evolution of defects. On the one hand, the proximity of surfaces accelerates the removal of point defects generated during implantation. Although there is some uncertainly in the specific value for the recombination length (or recombination probability) of point defects at surfaces, they are generally considered efficient sinks for point defects.[55] The proximity of defects to surfaces favors their rapid annihilation and the fast recovery of equilibrium conditions even with lower thermal budgets.[56] On the other hand, the atomic discontinuity at free surfaces or interfaces makes the atomic rearrangement of *a*-regions near the interfaces slower, as analyzed in the previous section.

Transmission electron microscopy images evidence poor recrystallization in ultrathin-body Si devices both in planar and FinFET structures when the whole Si thickness has been amorphized.[30] This is becoming a pressing concern as poor regrowth degrades the device performance.[52,54] In Fig. 6 we illustrate the regrowth of a 14 nm thick fin structure oriented along ⟨110⟩ using MD calculations in a simulation cell containing 84 000 atoms. The amorphous phase is built by the accumulation of bond defects and Tersoff potential is used to describe the Si–Si interactions.[7] The lateral sides contain 3 ML of *a*-Si, and lateral periodic boundary conditions are used while the top and bottom sides are let free to allow for the volume change in *a*-Si. A crystalline seed is left at the bottom of the fin so that it can trigger SPER. The dynamics is followed by 9 ns at temperature just below melting of *a*-Si. Figure 6 shows that regrowth advances from the amorphous-crystalline interface, starting from the middle of the fin, but it is halted at the vertical interfaces because of the stability of bond defects at interfaces. Then, {111} planes start to form as the regrowth in this direction is slower than along ⟨110⟩ and ⟨100⟩ directions,[57] preventing a clean regrowth. The detailed atomistic evolution provided by MD simulations demands long computational times. The capability to simulate SPER shape evolution in continuum methods have been recently achieved using the level set approach, taking into account orientation dependence and curvature.[58]

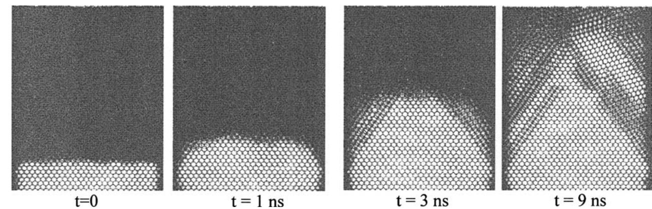

FIG. 6. Molecular dynamics simulations of the evolution of a 14 nm fin structure. A covering amorphous layer surrounds the Si fin. A crystalline seed is left at the bottom to promote solid-phase epitaxial regrowth. Poor regrowth causes {111} twin boundaries and polycrystalline Si.

IV. CONCLUSIONS

Process simulation capabilities must evolve to encompass processes, geometries, and materials considered for present and future devices. Detailed atomistic models are often too complicated or too slow to be used in actual process simulations but they are very useful to provide the physical understanding for the development of simplified models computationally more efficient. Ion implantation continues as the most promising technique to introduce dopants. Improved models have been developed to describe in detail dopant profiles, the kinetics of damage, and the interactions between dopants and defects. There is still a lot of room for improvement, specially related to the modeling of dopants in *a*-Si. Additional challenges arise in advanced architectures, such as FinFETs, because the introduction of highly tilted ions is quite inefficient and the regrowth of *a*-regions in narrow devices is hampered by the slow regrowth at the free interfaces and {111} planes. Although alternative materials, such as Ge or III-V compounds, are being considered for future technologies, a vast effort needs to be made to catch up with the mature knowledge of the Si material properties, technology, and modeling.

ACKNOWLEDGMENTS

This work has been partially funded by the Spanish Government under Project No. TEC2008-06069 and by Junta de Castilla y León under Project No. VA011A09.

[1]International Technology Roadmap for Semiconductors (www.itrs.net).
[2]M. S. Ameen, L. M. Rubin, M. A. Harris, and C. Huynh, J. Vac. Sci. Technol. B **26**, 373 (2008).
[3]K. Mistry *et al.*, Dig. Tech. Pap. - Symp. VLSI Technol. **2004**, 50.
[4]R. Lindsay *et al.*, Mater. Res. Soc. Symp. Proc. **765**, D7.4 (2003).
[5]N. Goel *et al.*, Tech. Dig. - Int. Electron Devices Meet. **2008**, 363.
[6]L. A. Marques, L. Pelaz, P. Lopez, M. Aboy, I. Santos, and J. Barbolla, Mater. Sci. Eng., B **124–125**, 72 (2005).
[7]J. Tersoff, Phys. Rev. B **39**, 5566 (1989).
[8]S. J. Cook and P. Clancy, Phys. Rev. B **47**, 7686 (1993).
[9]C. Krzeminski, Q. Brulin, V. Cuny, E. Lecat, E. Lampin, and F. Cleri, J. Appl. Phys. **101**, 123506 (2007).
[10]K. L. Saenger *et al.*, Mater. Res. Soc. Symp. Proc. **1070**, 205 (2008).
[11]M. D. Giles, J. Electrochem. Soc. **138**, 1160 (1991).
[12]G. Hobler, L. Pelaz, and C. S. Rafferty, J. Electrochem. Soc. **147**, 3494 (2000).

[13]D. G. Ashworth, R. Oven, and B. Mundin, J. Phys. D: Appl. Phys. **23**, 870 (1990).
[14]G. M. Yu, P. B. Griffin, and J. D. Plummer, Tech. Dig. - Int. Electron Devices Meet. **1998**, 717.
[15]M. T. Robinson and I. M. Torrens, Phys. Rev. B **9**, 5008 (1974).
[16]J. F. Ziegler, *The Stopping and Range of Ions in Solids* (Pergamon, New York, 1977), Vol. 1.
[17]M. Posselt and J. P. Biersack, Nucl. Instrum. Methods Phys. Res. B **64**, 706 (1992).
[18]G. Hobler, Nucl. Instrum. Methods Phys. Res. B **96**, 155 (1995).
[19]J. M. Hernandez-Mangas, J. Arias, L. Bailón, M. Jaraiz, and J. Barbolla, J. Appl. Phys. **91**, 658 (2002).
[20]M. J. Caturla, T. Diaz de la Rubia, L. A. Marques, and G. H. Gilmer, Phys. Rev. B **54**, 16683 (1996).
[21]P. Sigmund, Appl. Phys. Lett. **14**, 114 (1969).
[22]I. Santos, L. A. Marques, and L. Pelaz, Phys. Rev. B **74**, 174115 (2006).
[23]L. A. Marques, L. Pelaz, and I. Santos, Phys. Rev. B **74**, 201201 (2006).
[24]M. Posselt, Mater. Sci. Semicond. Process. **3**, 317 (2000).
[25]I. Santos, L. A. Marques, L. Pelaz, and P. Lopez, J. Appl. Phys. **105**, 083530 (2009).
[26]L. Pelaz, L. A. Marques, and J. Barbolla, J. Appl. Phys. **96**, 5947 (2004).
[27]G. Hobler and G. Otto, Mater. Sci. Semicond. Process. **6**, 1 (2003).
[28]J. A. van den Berg, S. Zhang, S. Whelan, D. G. Armour, R. D. Goldberg, P. Bailey, and T. C. Q. Noakes, Nucl. Instrum. Methods Phys. Res. B **183**, 154 (2001).
[29]Y. Kunni, M. Tabe, and K. Kakiyama, J. Appl. Phys. **56**, 279 (1984).
[30]R. Duffy, M. J. H. van Dal, B. J. Pawlak, M. Kaiser, R. G. R. Weemaes, B. Degroote, E. Lunnen, and E. Altamirano, Appl. Phys. Lett. **90**, 241912 (2007).
[31]P. Pichler, *Intrinsic Point Defects, Impurities and their Diffusion in Silicon* (Springer, Wien, 2004).
[32]M. Aboy, L. Pelaz, L. A. Marques, P. Lopez, J. Barbolla, and R. Duffy, J. Appl. Phys. **97**, 103520 (2005).
[33]K. Suzuki, Y. Kataoka, S. Nagayama, C. W. Magee, T. H. Buyuklimanli, and T. Nagayama, IEEE Trans. Electron Devices **54**, 262 (2007).
[34]R. Duffy *et al.*, Appl. Phys. Lett. **84**, 4283 (2004).
[35]V. C. Venezia, R. Duffy, L. Pelaz, M. J. P. Hopstaken, G. C. J. Maas, T. Dao, Y. Tamminga, and P. Graat, Mater. Sci. Eng., B **124–125**, 245 (2005).
[36]S. Mirabella, D. de Salvador, E. Bruno, E. Napolitani, E. F. Pecora, S. Boninelli, and F. Priolo, Phys. Rev. Lett. **100**, 155901 (2008).
[37]A. Mattoni and L. Colombo, Phys. Rev. B **69**, 045204 (2004).
[38]S. H. Jain, P. B. Griffin, J. D. Plummer, S. Mccoy, J. Gelpey, T. Selinger, and D. F. Downey, J. Appl. Phys. **96**, 7357 (2004).
[39]R. Duffy, V. C. Venezia, A. Heringa, M. J. P. Hopstaken, G. C. J. Maas, T. Dao, Y. Tamminga, and F. Roozeboom, Mater. Res. Soc. Symp. Proc. **810**, 437 (2005).
[40]M. J. P. Hopstaken, Y. Tamminga, M. A. Verheijen, R. Duffy, V. C. Venezia, and A. Heringa, Appl. Surf. Sci. **231–232**, 688 (2004).
[41]G. Impellizzeri, S. Mirabella, F. Priolo, E. Napolitani, and A. Carnera, J. Appl. Phys. **99**, 103510 (2006).
[42]M. Diebel and S. T. Dunham, Phys. Rev. Lett. **93**, 245901 (2004).
[43]S. Boninelli, G. Impellizzeri, S. Mirabella, F. Priolo, E. Napolitani, N. Cherkashin, and F. Cristiano, Appl. Phys. Lett. **93**, 061906 (2008).
[44]J. Kedzierski, M. Ieong, E. Novak, T. S. Kanarsky, Y. Zhang, D. Boyd, D. Fried, and H.-S. Philip Wong, IEEE Trans. Electron Devices **50**, 952 (2003).
[45]N. Collaert *et al.*, Solid-State Electron. **52**, 1291 (2008).
[46]M. J. H. van Dal *et al.*, Dig. Tech. Pap. - Symp. VLSI Technol. **2007**, 110.
[47]V. Subramanian *et al.*, Solid-State Electron. **51**, 551 (2007).
[48]H.-J. Gossmann, A. Agarwal, T. Parrill, L. M. Rubin, and J. M. Poate, IEEE Trans. Nanotechnol. **2**, 285 (2003).
[49]S. Takeuchi, N. D. Nguyen, F. E. Leys, R. Loo, T. Conard, W. Vandervorst, and M. Caymax, ECS Meeting Abstracts, 2008 (unpublished), Vol. 802, p. 2432.
[50]Y. Sasaki, K. Okashita, K. Nakamoto, T. Kitaoka, B. Mizuno, and M. Ogura, Tech. Dig. - Int. Electron Devices Meet. **2008**, 917.
[51]R. Duffy, G. Curatola, B. J. Pawlak, G. Doornbos, K. van der Tak, P. Breimer, J. G. M. van Berkum, and F. Roozeboom, J. Vac. Sci. Technol. B **26**, 402 (2008).
[52]L. Pelaz *et al.*, Tech. Dig. - Int. Electron Devices Meet. **2008**, 535.
[53]W. Vandervorst *et al.*, Ion Implantation Technology Conference Proceedings, 2008 (unpublished), Vol. 1066, pp. 446–456.
[54]M. J. H. van Dal, R. Duffy, B. J. Pawlak, N. Collaert, M. Jurczak, and R. J. P. Lander, Mater. Res. Soc. Symp. Proc. **1070**, 67 (2008).
[55]L. Pelaz, M. Aboy, P. Lopez, and L. A. Marques, J. Vac. Sci. Technol. B **24**, 2432 (2006).
[56]M. Aboy, L. Pelaz, L. A. Marques, L. Enriquez, and J. Barbolla, J. Appl. Phys. **94**, 1013 (2003).
[57]L. Csepregi, E. F. Kennedy, J. W. Mayer, and T. W. Sigmon, J. Appl. Phys. **49**, 3906 (1978).
[58]S. Morarka, N. G. Rudawski, and M. E. Law, J. Vac. Sci. Technol. B **26**, 357 (2008).